

UCSF

UC San Francisco Electronic Theses and Dissertations

Title

Solving the Structure of eIF2 Bound to eIF2B Using Cryogenic Electron Microscopy

Permalink

<https://escholarship.org/uc/item/00z4g4cg>

Author

Kenner, Lillian

Publication Date

2019

Peer reviewed|Thesis/dissertation

Solving the Structure of eIF2 Bound to eIF2B Using Cryogenic Electron Microscopy

by
Lillian Rose Kenner

DISSERTATION

Submitted in partial satisfaction of the requirements for degree of
DOCTOR OF PHILOSOPHY

in

Biophysics

in the

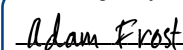
GRADUATE DIVISION

of the

UNIVERSITY OF CALIFORNIA, SAN FRANCISCO

Approved:

DocuSigned by:

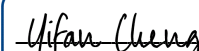


Adam Frost

2BFC3B4CEA6C478...

Chair

DocuSigned by:



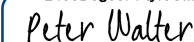
Yifan Cheng

DocuSigned by:




Mark von Zastrow

DocuSigned by:



Peter Walter

DocuSigned by:



Geeta Narlikar

EE2E6D32EE3043B...

Committee Members

Copyright 2019

by

Lillian Rose Kenner

Solving the Structure of eIF2 Bound to eIF2B Using Cryogenic Electron Microscopy

by

Lillian Rose Kenner

Abstract

Translation begins when initiation factor-2 (eIF2) delivers methionyl initiator tRNA (Met-tRNA_i) to the ribosome. The exchange of GDP bound to eIF2 for GTP is a prerequisite to binding Met-tRNA_i and is mediated by a second initiation factor, eIF2B. Regulation of mRNA translation is achieved through phosphorylation of eIF2 α at Ser51 which converts eIF2 from a substrate into a competitive inhibitor of eIF2B. Using the latest cryo-electron microscopy (cryoEM) technologies in both collection and data processing we were able to obtain three high resolution structures to interrogate the structural basis of the integrated stress response.

Here we discuss the structures of eIF2 bound to eIF2B as well as two eIF2s bound to eIF2B, and S51 phosphorylated eIF2 α bound to eIF2B. These structures were determined to fulfill these two goals, 1) how eIF2 binds to eIF2B for productive nucleotide exchange; and 2) how ISR-driven phosphorylation of eIF2 changes its binding.

The three structures discussed here have been solved by cryoEM. CryoEM is a high resolution technique for visualizing radiation-sensitive specimens like biological macromolecules. Recent advances of cryo-EM are provided by two major innovations. One is the employment of direct electron detector which can detect electrons directly and read them at high frame rate without a mechanical shutter. The other is motion correction, which compensates for the blurring effect of beam-induced motion. These two technologies have led to a “resolution

revolution” in cryoEM. Utilizing the most up to date software and hardware available through UCSF we were able to solve the structures of three protein complexes which were previously unattainable.

The first two structures of non-phosphorylated eIF2 bound to eIF2B reveal the mechanism for nucleotide turnover of eIF2. Similar to other G proteins, eIF2 switches between active GTP and inactive GDP bound states. Each round of nucleotide exchange of GDP to GTP on eIF2 by eIF2B reinitiates the eIF2 cycle that is essential for continued protein translation. The structural requirements of how eIF2B exchanges nucleotide on eIF2 have never been fully described. Here we observe that the two faces of eIF2B ϵ splay open the eIF2 γ GTP/GDP binding site allowing GDP release. Given the lack of direct interaction between the HEAT domain of eIF2B ϵ with the relevant areas of nucleotide exchange of the eIF2 γ subunit, we proposed that G domain nucleotide exchange is modulated through an allosteric interaction with the HEAT domain. C-terminal of the HEAT domain, eIF2B ϵ core at N258 and D262 binds the P-Loop of eIF2 γ through electrostatic contacts with R75.

The third structure is of S51 phosphorylated eIF2 α bound to eIF2B. Here we propose the mechanistic basis of how phosphorylation converts eIF2 from substrate to inhibitor of eIF2B. In eIF2 α P, the rearrangement of the S-loop derives from an intramolecular electrostatic interaction between Arg63 and Arg53 and the phosphate, which also exposes a hydrophobic surface upon phosphorylation-induced refolding. Through these interactions eIF2 α -P adopts a new conformation which suggests how the S-loop may become incompatible for binding to the site where non-phosphorylated eIF2 α binds as a substrate. This new binding mode is nonproductive for nucleotide exchange on eIF2-P and likely sequesters the catalytic domains into an inhibited

state that prevents the catalytic moieties of eIF2B ϵ from properly engaging in productive nucleotide exchange.

Table of Contents

eIF2B-catalyzed nucleotide exchange and phosphoregulation by the integrated stress response

Contributing authors	1
Abstract	1
Introduction	2
Results	3
eIF2B heterodecamer bound to one or two eIF2 heterotrimers	3
The bipartite basis of eIF2a recognition and assembly-stimulated activity	8
The structural basis of phosphoregulation by the ISR	10
Discussion	12
Materials and Methods	13
Purification of decameric eIF2B($\alpha\beta\gamma\delta\epsilon$)	14
Purification of heterotrimeric human eIF2	15
Purification of human eIF2 α	17
Purification of phosphorylated human eIF2 α	17
Purification of tetrameric eIF2B($\beta\gamma\delta\epsilon$)	17
Cloning of mutant eIF2B expression plasmids	18
EM sample preparation and data collection for ISRIB-bound eIF2•eIF2B and eIF2 α •eIF2B complexes	18
Image analysis and 3D reconstruction	19
Atomic modeling and validation	20

GDP exchange assay	21
Negative Stain collection and 2D Classification	22
References	23

List of figures

eIF2B-catalyzed nucleotide exchange and phosphoregulation by the integrated stress response

- Figure 1. eIF2B heterodecamer bound to one or two eIF2 heterotrimers. 5
- Figure 2. The bipartite basis of guanine nucleotide exchange by eIF2B. 6
- Figure 3. The bipartite basis of eIF2 α recognition and assembly-stimulated activity. 9
- Figure 4. The structural basis of phosphoregulation by the ISR. 11

Chapter I

eIF2B-catalyzed nucleotide exchange and phosphoregulation by the integrated stress response

Contributing authors

Lillian R. Kenner^{1†}, Aditya A. Anand^{1,2†}, Henry C. Nguyen¹, Alexander G. Myasnikov¹, Carolin J. Klose^{1,2}, Lea A. McGeever^{1,2}, Jordan C. Tsai^{1,2}, Lakshmi E. Miller-Vedam¹, Peter Walter^{1,2,*}, Adam Frost^{1,3,*}

¹Department of Biochemistry and Biophysics, University of California at San Francisco, San Francisco, CA, USA

²Howard Hughes Medical Institute

³Chan Zuckerberg Biohub, San Francisco, CA, USA

†These authors contributed equally

Abstract

The integrated stress response (ISR) tunes the rate of protein synthesis. Control is exerted by phosphorylation of the general translation initiation factor eIF2. eIF2 is a guanosine triphosphatase that becomes activated by eIF2B, a two-fold symmetric and heterodecameric complex that functions as eIF2's dedicated nucleotide exchange factor. Phosphorylation converts eIF2 from a substrate into an inhibitor of eIF2B. We report cryo-electron microscopy structures of eIF2 bound to eIF2B in the dephosphorylated state. The structures reveal that the eIF2B

decamer is a static platform upon which one or two flexible eIF2 trimers bind and align with eIF2B's bipartite catalytic centers to catalyze nucleotide exchange. Phosphorylation refolds eIF2a, allowing it to contact eIF2B at a different interface and, we surmise, thereby sequestering it into a nonproductive complex.

Introduction

Numerous factors regulate translation of the genetic code into proteins, including eukaryotic translation initiation factor 2 (eIF2), a guanosine triphosphatase (GTPase) composed of a, b, and g subunits. During initiation, eIF2 binds tRNA^{Met} and GTP to form a ternary complex that scans mRNAs for start codons. After start codon detection, eIF2g hydrolyzes its GTP and translation initiates. For eIF2 reactivation, guanosine diphosphate (GDP) is replaced by GTP upon catalysis by a dedicated guanine nucleotide exchange factor (GEF), eIF2B. eIF2 and eIF2B control translation initiation. Stress-responsive kinases phosphorylate eIF2a at the conserved residue Ser51, transforming eIF2 from substrate into a competitive GEF inhibitor. Phosphoregulation of eIF2 is known as the integrated stress response (ISR) (1). Once activated, the ISR reduces overall protein synthesis while enhancing translation of a small subset of mRNAs in response to cellular threats, including protein misfolding, infection, inflammation, and starvation (1–3). eIF2B comprises two copies each of an a, b, g, d, and e subunit that assemble into a two-fold symmetric heterodecamer (4, 5). The eIF2Be subunit contains the enzyme's catalytic center and associates closely with eIF2Bg. Two copies each of the eIF2Bb and eIF2Bd subunits form the complex's core, bridged by two eIF2Ba subunits across the symmetry interface (4, 6). Genetic and biochemical studies have identified residues responsible

for eIF2B's catalytic activity and have suggested how eIF2 binding to eIF2B may differ after eIF2a Ser51 phosphorylation (4, 7–10). Yet it has remained unknown how eIF2 recognizes eIF2B, how eIF2B catalyzes nucleotide exchange, or how eIF2 transforms from a substrate to a high-affinity inhibitor of eIF2B after its phosphorylation. A potent small-molecule, drug-like inhibitor of the integrated stress response, ISRIB, allays the effects of eIF2a phosphorylation by activating eIF2B (11–13). Upon adding ISRIB, cells undergoing the ISR resume translation (12, 13). When administered to rodents, ISRIB enhances cognition and ameliorates cognitive deficits caused by traumatic brain injury and prioninduced neurodegeneration (15). Furthermore, eIF2B activation rescues cognitive and motor function in mouse models of leukoencephalopathy with vanishing white matter disease (VWMD), a fatal familial disorder associated with mutations spread over all eIF2B subunits (16). ISRIB bridges the symmetric interface of two eIF2B subcomplexes to enhance the formation of the decameric eIF2B holoenzyme (17, 18), enhancing available GEF activity by promoting higher-order assembly of the eIF2B decamer. However, it has remained an enigma why decameric eIF2B would be more active than its unassembled subcomplexes. To explore this question, we determined structures of eIF2B bound with both its substrate, eIF2 (a,b,g), and its inhibitor, eIF2a•P.

Results

eIF2B heterodecamer bound to one or two eIF2 heterotrimers

We coexpressed all five subunits of human eIF2B in *Escherichia coli* and all three subunits of human eIF2 in *Saccharomyces cerevisiae* (fig. S1, A and B). The yeast expression

strain lacked GCN2, an eIF2 kinase, to ensure expression of homogeneously nonphosphorylated eIF2 (19). We incubated ISRIB and purified eIF2 at concentrations near the Michaelis constant of the nucleotide exchange reaction [$K_m = \sim 1.5$ mM (17)] and added an inter-amine cross-linker to stabilize complexes before sample vitrification and cryo-electron microscopy (cryo-EM) analysis (fig. S2, A to C). We resolved two structures: eIF2B bound asymmetrically to a single eIF2 trimer and eIF2B bound symmetrically to two eIF2 trimers (Fig. 1, figs. S3A, S4, and S5, and tables S1 to S3). Snaking across the surface of eIF2B, we observed density consistent in size and shape with eIF2 subunits and the previously unresolved eIF2Be HEAT domain. Comparison with homologous structures of eIF2a and eIF2g revealed that the assembled eIF2•eIF2B complex retained similarity to the structures of these individually analyzed domains (20–22) (Fig. 2 and fig. S6). We resolved only a single helix of eIF2b (Fig. 1, A and D, and Fig. 2A), consistent with other studies (20, 21). In both reconstructions, all five subunits of eIF2B can be superimposed on previously determined structures lacking eIF2 [root mean square deviation (RMSD) ≈ 0.6 Å] (17). Thus, eIF2B retained its overall arrangement when bound to one or two eIF2s (Fig. 1), indicating that eIF2 binds via equivalent modes to both sides of a static eIF2B scaffold with no allostery in eIF2B upon eIF2 engagement. This is consistent with noncooperative kinetics reported for nucleotide exchange by eIF2B decamers (17).

Fig. 1

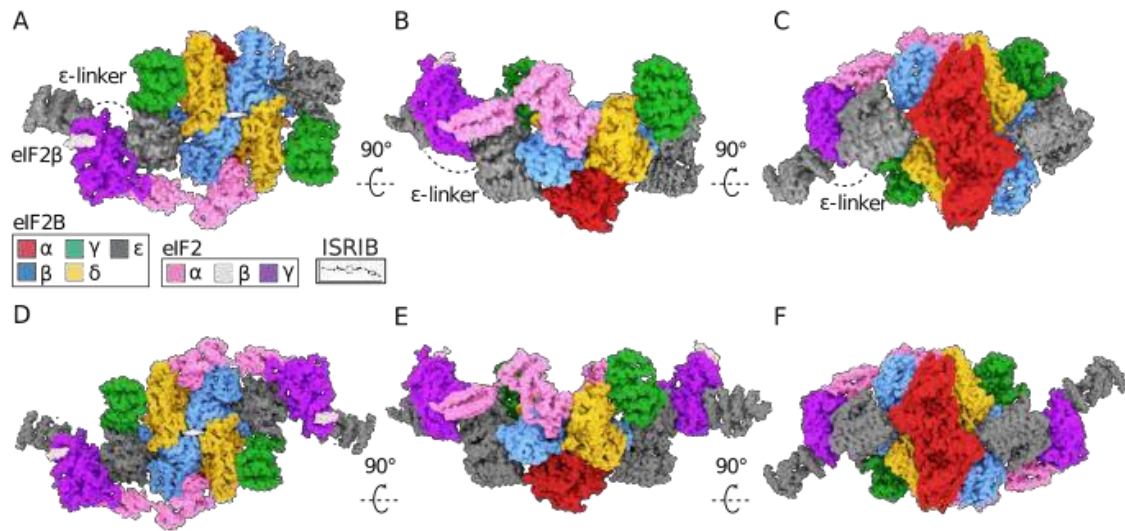


Fig. 1 eIF2B heterodecamer bound to one or two eIF2 heterotrimers. (A to C) Orthogonal views of a single elongated eIF2 heterotrimer bound to ISRIB-stabilized eIF2B decamers. ISRIB density is rendered in white. (D to F) Orthogonal views of a pair of elongated eIF2 heterotrimers bound to ISRIB-stabilized eIF2B decamers. ISRIB density is rendered in white.

Bound to eIF2B, eIF2 adopted an extended 150 Å conformation (Figs. 1 and 2A) with eIF2's central nucleotide-binding g subunit flanked by its a and b subunits at its opposing ends. eIF2g contains classical GTP-binding motifs, including the nucleobase-binding G4 motif, the phosphate-binding P-loop, and switch helices 1 and 2. eIF2B recognizes eIF2 via coincident binding of both eIF2a and eIF2g. Binding to both eIF2 subunits involves bipartite elements of eIF2B (Fig. 1 and Fig. 2, A to C).

Figure 2

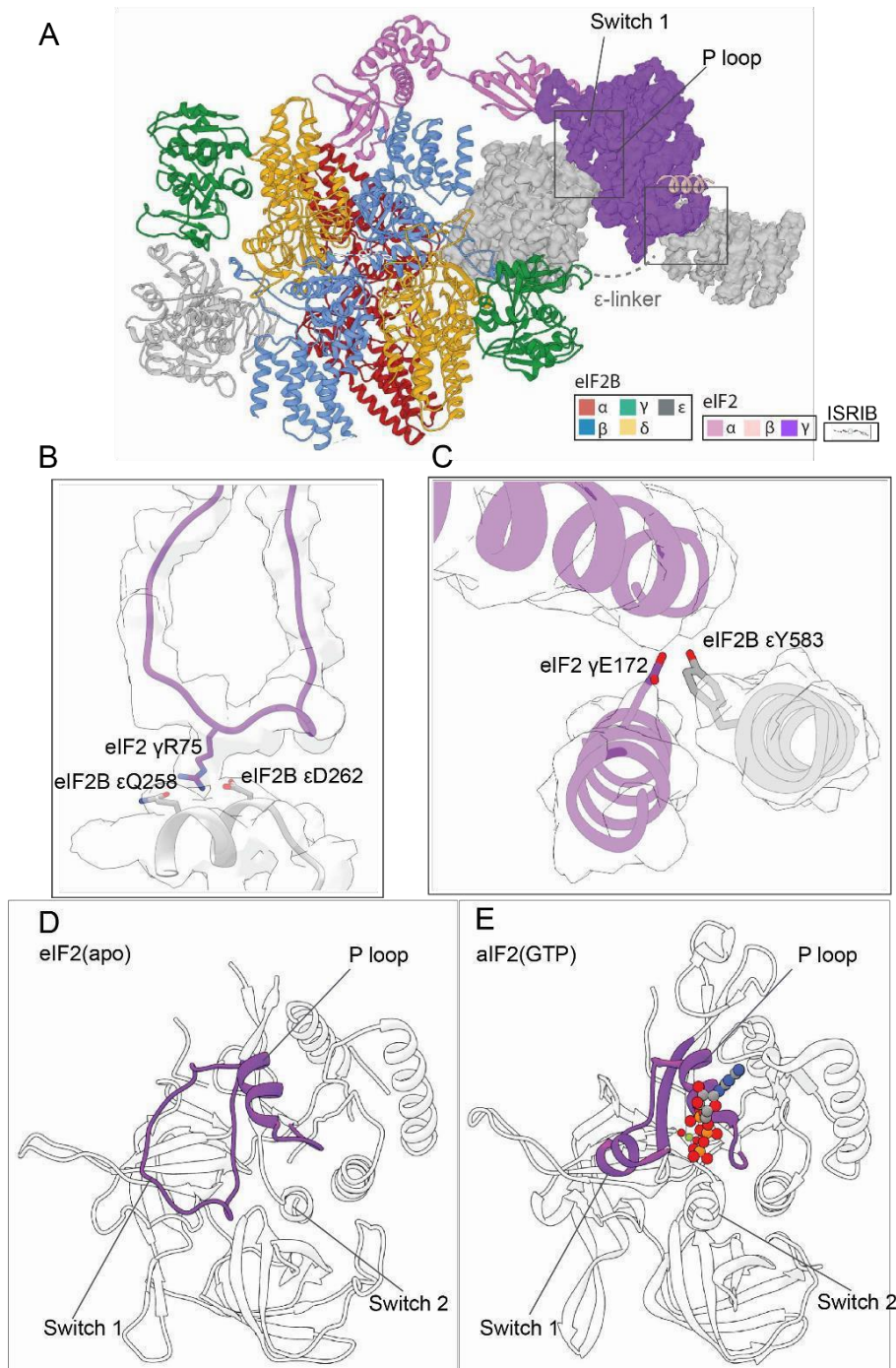


Fig. 2 The bipartite basis of guanine nucleotide exchange by eIF2B.

(A) Structural model of a single eIF2 heterotrimer bound to the eIF2B decamer, emphasizing the cryo-EM density for eIF2 γ and its interactions with eIF2B ϵ . (B) Switch 1 of eIF2 γ stabilized as an open loop due to interactions between R75 eIF2 γ and Q258 and D262 of eIF2B ϵ . (C) Y583 from the HEAT domain of eIF2B ϵ (one helix shown) contacting eIF2 γ E172. (D and E)

Comparison of the open, nucleotide-free state of eIF2 reported here (D) and an aIF2 structure bound to GTP (PDB: 4RCY) (E). Amino acid abbreviations: D, Asp; E, Glu; Q, Gln; R, Arg; Y, Tyr.

First, bipartite recognition of eIF2g involves two domains of eIF2Be that function together to splay open the nucleotide-binding site. Our nucleotide-free cryo-EM model is similar to the g subunit of GTP-bound aIF2 from *Sulfolobus solfataricus* (23) (Fig. 2, D and E; average RMSD \approx 2.3 Å). However, surrounding the GTP-binding pocket, the structures diverged considerably, with the P-loop in eIF2B•eIF2 partially occluding the nucleotide-binding site (RMSD \approx 12 Å). Prior work implicated the HEAT domain in catalysis (23–26). In agreement with those findings, eIF2g interacts with the HEAT domain, including a partially hydrophobic surface that includes eIF2Be Tyr583 (Fig. 2C). On the opposing side of the nucleotide-binding pocket, the central core of eIF2Be engaged with an open-loop conformation of switch 1. This change appears to be due to electrostatic interactions between eIF2g Arg75 in switch 1 and Gln258 and Asp262 in eIF2Be (Fig. 2B). Thus, both eIF2Be's HEAT domain and core collaborate to open the nucleotidebinding site (Fig. 2, B to D). The second example of bipartite recognition concerns eIF2a binding in the cleft between eIF2Bb and eIF2Bd' (d' denotes the d subunit) Notably, this binding site only exists when two tetramers of eIF2B (bgde) associate to form the symmetry interface in octameric eIF2B (bgde)₂. eIF2a contains two structured domains separated by a flexible linker (Figs. 1 and 2 and fig. S6).

The bipartite basis of eIF2a recognition and assembly-stimulated activity

The N terminus consists of an OB-fold, common in tRNA-binding proteins (20). The OB-fold is further elaborated with a positively charged loop (the S-loop), while the C-terminal ab-fold connects eIF2a to eIF2g. The S-loop harbors Ser51 and is responsible for all of the resolvable contacts between eIF2a and eIF2B's b subunit (Fig. 3A). Prior work implicated a conserved "79KGYID83" (Lys79-Gly80-Tyr81-Ile82-Asp83) motif in eIF2a as being important for eIF2B binding (10). Of note, an interaction between Tyr81 was well resolved adjacent to the equally prominent Arg250 on eIF2Bd' (Fig. 3B). When we mutated Arg250 to either alanine (R250A) or glutamate (R250E), neither mutation affected the residual GEF activity displayed by dissociated tetramers (Fig. 3D; R250A $k_{obs} = 0.013 \text{ min}^{-1}$, R250E $k_{obs} = 0.023 \text{ min}^{-1}$, wild-type $k_{obs} = 0.016 \text{ min}^{-1}$), whereas both mutants diminished the GEF activity of the ISRIB-stabilized eIF2B octamer when compared to the wild type (Fig. 3E; R250A $k_{obs} = 0.012 \text{ min}^{-1}$, R250E $k_{obs} = 0.017 \text{ min}^{-1}$, wild-type $k_{obs} = 0.063 \text{ min}^{-1}$). This is consistent with the notion that unphosphorylated eIF2a interacts with the trans tetramer only upon assembly of octameric or decameric eIF2B across its symmetry interface. On the cis tetramer, eIF2a's positively charged S-loop binds negatively charged and polar residues along the exposed surface of eIF2Bb. This binding site is consistent with yeast studies suggesting that mutations in this site compromise eIF2 binding (7).

Fig. 3

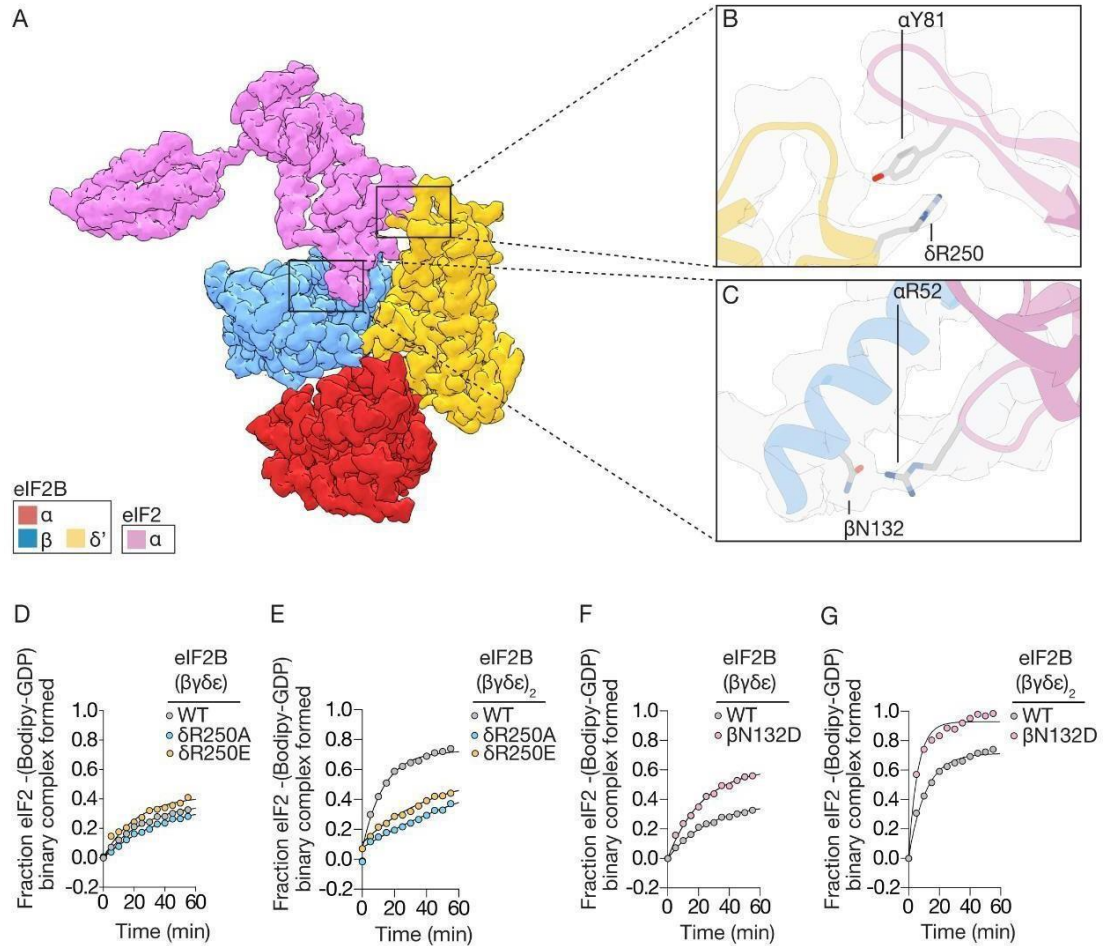


Fig. 3 The bipartite basis of eIF2 α recognition and assembly-stimulated activity. (A) Cryo-EM density for eIF2 α bound to the regulatory subcomplex (α , β , δ , or RSC) of eIF2B. (B) Density and zoom-in detail of a cation- π interaction between eIF2B δ and eIF2 α . (C) Polar interactions between eIF2B β and the S-loop of eIF2 α . (D and F) GEF activity of wild-type versus mutated eIF2B ($\beta\gamma\delta\epsilon$) tetramers measured by BODIPY-labeled GDP fluorescence unquenching. (E and G) ISRIB-stabilized eIF2B ($\beta\gamma\delta\epsilon$)₂ octamers measured by BODIPY-labeled GDP fluorescence unquenching. A, Ala; N, Asn.

Examination of the structure identified a potential hydrogen bond between eIF2B β

Asn132 and eIF2 α Arg52 (Fig. 3C). We substituted Asn132 with aspartate (N132D), anticipating

that the introduced charge complementarity would enhance binding to eIF2a Arg52. When compared to wild-type eIF2B tetramers, eIF2B-bN132D tetramers and ISRIB-stabilized octamers indeed proved to be gain-of-function mutations, exhibiting enhanced GEF activity by a factor of ~2 [Fig. 3, F and G, and fig. S1D; eIF2B (bgde) bN132D $k_{obs} = 0.044 \text{ min}^{-1}$, eIF2B (bgde)₂ bN132D $k_{obs} = 0.169 \text{ min}^{-1}$]. This is consistent with eIF2B tetramers possessing reduced activity relative to assembled octameric or decameric holo-eIF2B. eIF2a binding in the cleft between tetramers further supports the notion that ISRIB enhances eIF2B's GEF activity by promoting higher-order assembly.

The structural basis of phosphoregulation by the ISR

To understand how eIF2a phosphorylation on Ser51 transforms eIF2 from substrate to inhibitor, we coexpressed the isolated eIF2a subunit in *E. coli* with the kinase domain of PERK (doublestranded RNA-activated protein kinase-like ER kinase), an eIF2 kinase (fig. S1C). We incubated preassembled eIF2B decamers with an excess of eIF2a-P, followed by cross-linking and vitrification. Reconstruction of the eIF2B decamer adorned with two copies of eIF2a-P (Fig. 4A, figs. S7 and S8, and tables S1 to S3) revealed eIF2a-P bridging the interface between eIF2Bd and eIF2Ba (Fig. 4A).

Fig. 4

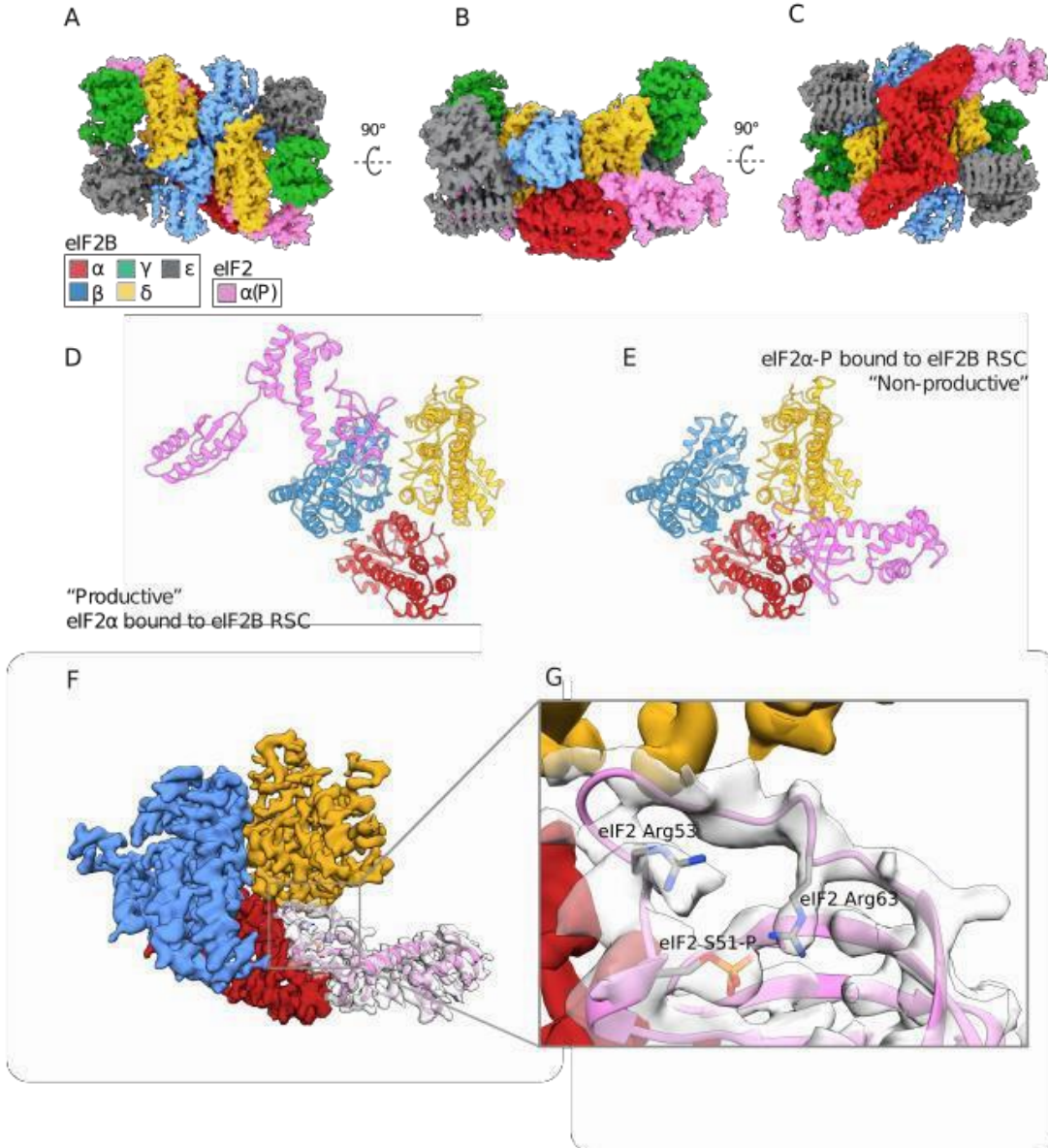


Fig. 4 The structural basis of phosphoregulation by the ISR.

(A to C) Orthogonal views of a pair of Ser⁵¹-phosphorylated eIF2α subunits bound to the eIF2B decamer. (D) The productive binding mode of nonphosphorylated eIF2α. (E) The nonproductive and nonoverlapping binding mode of phosphorylated eIF2α. (F) Cryo-EM density of phosphorylated eIF2α bound to the regulatory subcomplex (α, β, δ) of eIF2B. (G) Zoom-in of the S-Loop cryo-EM density and model, placing the Ser⁵¹ phosphate moiety near eIF2α Arg⁵³ and Arg⁶³.

Intriguingly, we observed no overlap between the binding sites of nonphosphorylated eIF2a described above and eIF2a-P (Fig. 4, B and C). Density for both eIF2a Ser51-P and two arginines positioned ~ 4 Å away, eIF2a Arg53 and Arg63, were well resolved and suggestive of an electrostatic coordination responsible for phosphorylation-induced refolding of the S-loop (Fig. 4, F and G, fig. S8, and movie S1), as initially observed by Kashiwagi et al. (27). The phosphorylation-induced rearrangement also positions hydrophobic residues on eIF2a for potential interactions with hydrophobic residues on eIF2B (including eIF2a Ile55, Ile58, and Leu61 and eIF2Bd Leu314, Ala315, Ala318, and Phe322). This structural model agrees with analyses in yeast and mammalian systems. eIF2Ba is dispensable for viability in yeast, yet eIF2Ba deletion impairs phospho-inhibition of eIF2B, consistent with the subunit's role in binding eIF2a-P (28). Point mutations with identical phenotypes cluster at the interface between eIF2Ba and eIF2Bd (e.g., eIF2Ba Phe239 and eIF2Bd Met506 and Pro508) (29, 30). eIF2Bd Leu314 complements the hydrophobic surface of the eIF2a S-loop that is exposed upon refolding, and mutation of Leu to Gln at the equivalent position in *S. cerevisiae*, L381Q, impairs the ISR in yeast (29). These data validate the phosphorylation-induced refolding and relocation of eIF2a-P observed here.

Discussion

Our analyses reveal the mechanistic basis of eIF2B's nucleotide exchange activity and suggest how phosphorylation converts eIF2 from substrate to inhibitor. The nonphosphorylated form of eIF2 binds to a composite surface created only in the assembled decamer, allowing both the core and the flexibly attached HEAT domain of eIF2Be to engage its target in concert for

enhanced GEF activity. By contrast, eIF2a-P adopts a new conformation and suggests how the S-loop may become incompatible for binding to the site where nonphosphorylated eIF2a binds as a substrate (movie S1). Phosphorylation thus enables a distinct binding mode on the opposite side of eIF2B where eIF2a-P lies exiled at the interface of eIF2Ba and eIF2Bd. In eIF2a•P, the rearrangement of the S-loop derives from an intramolecular electrostatic interaction between Arg63 and Arg53 and the phosphate, which also exposes a hydrophobic surface upon phosphorylation-induced refolding. We surmise that this new binding mode is nonproductive for nucleotide exchange on eIF2-P and sequesters the catalytic domains into an inhibited state that prevents the catalytic moieties of eIF2Be from properly engaging in productive nucleotide exchange.

Materials and Methods

Purification of decameric eIF2B($\alpha\beta\gamma\delta\epsilon$)₂

As previously described (17), pJT066, pJT073, and pJT074 were co-transformed into One Shot BL21 Star (DE3) chemically competent *E. coli* cells (Invitrogen) and grown in Luria broth containing ampicillin, kanamycin, and chloramphenicol at 37°C on an orbital shaker. When the culture reached an OD₆₀₀ of ~0.6, the temperature was reduced to 16°C, and the culture was induced with 0.8 mM IPTG (Gold Biotechnology) and grown for 16 hours. Cells were harvested and lysed with an EmulsiFlex-C3 (Avestin) in a buffer containing 20 mM HEPES-KOH, pH 7.5, 250 mM KCl, 1 mM tris(2-carboxyethyl)phosphine (TCEP), 5 mM MgCl₂, 15 mM imidazole, and complete EDTA-free protease inhibitor cocktail (Roche). The lysate was clarified at 30,000g

for 20 min at 4°C. Subsequent purification steps were conducted on the ÄKTA Pure (GE Healthcare) system at 4°C. The clarified lysate was loaded onto a HisTrap HP 5 ml, washed in binding buffer (20 mM HEPES-KOH, pH 7.5, 200 mM KCl, 1 mM TCEP, 5 mM MgCl₂, and 15 mM imidazole), and eluted with a linear gradient (75 ml) of 15 mM to 300 mM imidazole in the same buffer. The eIF2B fraction eluted from the HisTrap column at 80 mM imidazole. The eIF2B fraction was collected and loaded onto a 20 ml Mono Q HR16/10 column (GE Healthcare), washed in Buffer A (20 mM HEPES-KOH, pH 7.5, 200 mM KCl, 1 mM TCEP, and 5 mM MgCl₂) and eluted with a linear gradient (200 ml) of 200 mM to 500 mM KCl in the same buffer. The eIF2B fraction eluted off the Mono Q column at a conductivity of 46 mS/cm (corresponding to 390 mM KCl). Fractions were collected, concentrated with an Amicon Ultra-15 concentrator (EMD Millipore) with a 100,000-dalton molecular weight cutoff, and loaded onto a Superdex 200 10/300 GL column (GE Healthcare) equilibrated with Buffer A. A typical preparation yielded approximately 0.5 mg of eIF2B($\alpha\beta\gamma\delta\epsilon$)₂ from a 1-liter culture.

Purification of heterotrimeric human eIF2

Human eIF2 was prepared from an established recombinant *S. cerevisiae* expression protocol (19). In brief, the yeast strain GP6452 (gift from the Pavitt lab, University of Manchester) containing yeast expression plasmids for human eIF2 subunits and a deletion of GCN2 encoding the only eIF2 kinase in yeast, was grown to saturation in synthetic complete media (Sunrise Science Products) with auxotrophic markers (-Trp, -Leu, -Ura) in 2% dextrose. The β and α subunits of eIF2 were tagged with His6 and FLAG epitopes, respectively. A 12-liter yeast culture was grown in rich expression media containing yeast extract, peptone, 2%

galactose, and 0.2% dextrose. Cells were harvested and resuspended in lysis buffer [100 mM Tris, pH 8.5, 300 mM KCl, 5 mM MgCl₂, 0.1% NP-40, 5 mM imidazole, 10% glycerol (Thermo Fisher Scientific), 2 mM DTT, 1× protease inhibitor cocktail (Sigma Aldrich #11836170001), 1 µg/ml each aprotinin (Sigma Aldrich), leupeptin (Sigma Aldrich), pepstatin A (Sigma Aldrich)]. Cells were lysed in liquid nitrogen using a steel blender. The lysate was centrifuged at 10,000g for 1 hour at 4°C. Subsequent purification steps were conducted on the ÄKTA Pure (GE Healthcare) system at 4°C. Lysate was applied to a 5-ml HisTrap Crude column (Thermo Fisher Scientific) equilibrated in buffer (100 mM HEPES, pH 7.5, 100 mM KCl, 5 mM MgCl₂, 0.1% NP-40, 5% glycerol, 1 mM dithiothreitol, 0.5× protease inhibitor cocktail, 1 µg/ml each aprotinin, leupeptin, pepstatin A). eIF2 bound to the column, was washed with equilibration buffer and eluted using a 50 ml linear gradient of 5 mM to 500 mM imidazole. Eluted eIF2 was incubated with FLAG M2 magnetic affinity beads, washed with FLAG wash buffer (100 mM HEPES, pH 7.5, 100 mM KCl, 5 mM MgCl₂, 0.1% NP-40, 5% glycerol, 1 mM TCEP, 1× protease inhibitor cocktail, 13 µg/ml each aprotinin, leupeptin, pepstatin A) and eluted with FLAG elution buffer [identical to FLAG wash buffer but also containing 3× FLAG peptide (100 µg/ml, Sigma Aldrich)]. Concentration of purified protein was measured by BCA assay (Thermo Fisher Scientific # PI23225); protein was flash-frozen in liquid nitrogen and stored in elution buffer at -80° C. A typical preparation yielded 1 mg of eIF2 from a 12-liter culture.

Purification of human eIF2 α

Human eIF2 α was E. coli codon-optimized, synthesized and cloned into a pUC57 vector by GenScript Inc. PCR-amplified dsDNA fragments containing the eIF2 α sequence were cloned

into a pET28a vector using an In-Fusion HD Cloning Kit (Takara Bio), resulting in the kanamycin-resistant expression plasmid, pAA007. pAA007 was co-transformed into One Shot BL21 Star (DE3) chemically competent *E. coli* cells (Invitrogen), along with the tetracycline-inducible, chloramphenicol-resistant plasmid, pG-Tf2, containing the chaperones groES, groEL, and tig (Takara Bio). Transformed cells were grown in Luria broth containing kanamycin and chloramphenicol at 37°C on an orbital shaker. When the culture reached an OD₆₀₀ of ~0.2, 1 ng/mL tetracycline was added to induce expression of chaperones. At an OD₆₀₀ of ~0.8, the temperature was reduced to 16°C, eIF2 α expression was induced with 1 mM IPTG (Gold Biotechnology) and the culture was grown for 16 hours. Cells were harvested and lysed with an EmulsiFlex-C3 (Avestin) in a buffer containing 100 mM HEPES-KOH, pH 7.5, 300 mM KCl, 2 mM dithiothreitol (DTT), 5 mM MgCl₂, 5 mM imidazole, 10% glycerol, 0.1% NP-40, and complete EDTA-free protease inhibitor cocktail (Roche). The lysate was clarified at 10,000g for 60 min at 4°C. Subsequent purification steps were conducted on the ÄKTA Pure (GE Healthcare) system at 4°C. The clarified lysate was loaded onto a 5-ml HisTrap FF Crude column (GE Healthcare), washed in a buffer containing 20 mM HEPES-KOH, pH 7.5, 100 mM KCl, 5% glycerol, 1 mM DTT, 5 mM MgCl₂, 0.1% NP-40, and 20 mM imidazole, and eluted with 75-ml linear gradient of 20 to 500 mM imidazole. The eIF2 α containing fractions were then collected and applied to a MonoS HR 10/10 (GE Healthcare) equilibrated in a buffer containing 20 mM HEPES-KOH, pH 7.5, 100 mM KCl, 1 mM DTT, 5% glycerol, and 5 mM MgCl₂. The column was washed in the same buffer and eluted with a 75-mL linear gradient of 100 mM to 1 M KCl. eIF2 α containing fractions were collected and concentrated with an Amicon Ultra-15 concentrator (EMD Millipore) with a 30,000-dalton molecular mass cutoff and chromatographed

on a Superdex 75 10/300 GL (GE Healthcare) column equilibrated in a buffer containing 20 mM HEPES-KOH, pH 7.5, 100 mM KCl, 1 mM TCEP, 5 mM MgCl₂, and 5% glycerol. A typical preparation yielded approximately 2 mg of eIF2 α from a 1-liter culture.

Purification of phosphorylated human eIF2 α

eIF2 α was expressed and purified as above, but with the following modifications: One Shot BL21 Star (DE3) E. coli were co-transformed with pAA007, pG-Tf2, and a third plasmid expressing the kinase domain of PERK (PERK 4: PERKKD-pGEX4T-1, Addgene plasmid #21817 donated by Dr. David Ron) and a resistance marker towards ampicillin. Transformed bacteria were grown in Luria broth containing ampicillin, kanamycin, and chloramphenicol. For purification, 1x PhosSTOP (Roche) was added to the lysis and purification buffers. Phosphorylation was confirmed by Phos-Tag SDS-PAGE (Wako) as described previously (31), and by Western blot with an eIF2 α S51 phosphorylation-specific antibody (Cell Signaling, #9721).

Purification of tetrameric eIF2B($\beta\gamma\delta\epsilon$)

Tetrameric eIF2B($\beta\gamma\delta\epsilon$) and tetrameric eIF2B($\beta\gamma\delta\epsilon$) mutant proteins were purified using the same protocol as described for the decamer with the exception that expression strains were cotransformed without the eIF2B α subunit expressing plasmid. A typical preparation yielded approximately 0.75 mg of eIF2B($\beta\gamma\delta\epsilon$) from a 1-liter culture.

eIF2B($\beta\gamma\delta\epsilon$) tetramer with co-transformed plasmids: pJT073, pJT074 β N132D

eIF2B($\beta\gamma\delta\epsilon$) tetramer with co-transformed plasmids: pAA012, pJT074 δ R250A

eIF2B($\beta\gamma\delta\epsilon$) tetramer with co-transformed plasmids: pAA013, pJT074 δ R250E

eIF2B($\beta\gamma\delta\epsilon$) tetramer with co-transformed plasmids: pAA014, pJT074

Cloning of mutant eIF2B expression plasmids

Mutant eIF2B constructs were generated by site-directed mutagenesis on pJT073 for β and δ , and pJT066 for α , using the primer indicated and its reverse complement.

β N132D (pAA012): 5'-

CCACTACGCTCAGCTGCAGTCTGACATCATCGAAGCTATCAACG-3'

δ R250A (pAA013): 5'-

CCCCGCCGAACGAAGAACTGTCTGCTGACCTGGTTAACAACTGAAACCG-3'

δ R250E (pAA014): 5'-

CCCCGCCGAACGAAGAACTGTCTGAGGACCTGGTTAACAACTGAAACCG-3'

EM sample preparation and data collection for ISRIB-bound eIF2•eIF2B and eIF2 α •eIF2B complexes

Decameric eIF2B($\alpha\beta\gamma\delta\epsilon$)₂ + eIF2($\alpha\beta\gamma$) + ISRIB: eIF2B($\alpha\beta\gamma\delta\epsilon$)₂ was diluted to 800 nM eIF2B, eIF2 to 2 μ M, and a stock solution of 200 μ M ISRIB in N-methyl-2-pyrrolidone (NMP) was added to a final ISRIB concentration of 2 μ M in a final solution containing 20 mM HEPES-KOH, pH 7.5, 100 mM KCl, 1 mM TCEP, 5 mM MgCl₂, 0.1% NMP, and incubated on ice for 10 min. An inter-amine bifunctional crosslinker (Pierce premium BS3, #PG82084) was then added at a concentration of 0.25mM, and the mixture was incubated on ice for 2 hours before

quenching with 10mM Tris HCl. Decameric eIF2B($\alpha\beta\gamma\delta\epsilon$)₂ + eIF2 α (P): eIF2B($\alpha\beta\gamma\delta\epsilon$)₂ was diluted to 800 nM and eIF2 α (P) to 2.4 μ M in a final solution containing 20 mM HEPES-KOH, pH 7.5, 100 mM KCl, 1 mM TCEP, 5mM MgCl₂, 0.1% NMP, and incubated on ice for 10 min and cross-linked as described above. Each sample was applied to Quantifoil R 1.2/1.3 200 or 400 Au mesh grids (Quantifoil, Germany). Quantifoil grids were used without glow discharging. Using a Vitrobot Mark IV at 4°C and 100% humidity with Whatman Filter Paper 1, 3.5 μ l of sample was applied to the grid, incubated for an additional 10s, then blotted with 0 mm offset for ~6 s and plunge-frozen in liquid ethane. Two data sets were collected. Both data sets were collected with on a 300 kV Titan Krios at UCSF using a K2 Summit detector operated in superresolution mode; 3233 images for eIF2P•eIF2B and 3947 images for eIF2•eIF2B were collected at a magnification of 29,000x (0.41Å per super-resolution pixel, binned by a factor of 2 to 0.82Å for subsequent processing). Dose-fractionated stacks were collected according to the parameters in Table S1.

Image analysis and 3D reconstruction

All dose-fractionated image stacks were corrected for motion artifacts, 2 \times binned in the Fourier domain, and dose-weighted using MotionCor2 (32), resulting in one dose-weighted and one unweighted integrated image per stack with pixel sizes of 0.822 Å. The parameters of the contrast transfer function (CTF) were estimated using GCTF-v1.06 (33) and the motion-corrected but unweighted images; automated particle picking was done using Gautomatch-v0.53 and averaged in 2D using Cryosparc v0.6.5 (34). For the 3D reconstruction, an ab initio

reconstruction was done without symmetry, followed by homogeneous refinement. High-resolution homogeneous refinement was then performed in cryoSPARC, using dynamic masks and imposed C2 symmetry for 2 eIF2 bound to eIF2B, C1 symmetry was used for 1 eIF2 bound to eIF2B. These maps were low-pass filtered and sharpened in cryoSPARC. For eIF2 α -phospho bound to eIF2B, manual refinement with C2 symmetry and automated sharpening were performed in cisTEM (35). Molecular graphics and analyses were performed with the UCSF Chimera package. UCSF Chimera is developed by the Resource for Biocomputing, Visualization, and Informatics and supported by NIGMS P41-GM103311 (36). Accession numbers for the structures are as follows: EMD-0649, EMD-0651, EMD-0664 (density maps; Electron Microscopy Data Bank).

Atomic modeling and validation

For all models, previously determined structures of the human eIF2B complex [PDB: 6CAJ (17)], human eIF2 alpha [PDBs: 1Q8K (20) and 1KL9 (21)], the C-terminal HEAT domain of eIF2B epsilon [PDB: 3JUI (26)], and mammalian eIF2 gamma [PDB: 5K0Y (37)] were used for initial atomic interpretation. The models were manually adjusted and rebuilt in Coot (38) and then refined in phenix.real_space_refine (39) using global minimization, morphing, secondary structure restraints, Ramachandran restraints, and local grid search. Then iterative cycles of manually rebuilding in Coot and phenix.real_space_refine with additionally B-factor refinement were performed. The final model statistics were tabulated using Molprobit (40) (Table S3). Map versus atomic model FSC plots were computed after masking using EMAN2 (41) and using calculated density maps from e2pdb2mrc.py with heteroatoms (ISRIB)

and per-residue B-factor weighting. Solvent accessible surfaces and buried surface areas were calculated from the atomic models using UCSF Chimera. Final atomic models have been deposited at the PDB with the following accession codes: 1 eIF2•eIF2B•ISRIB (6O81); 2 eIF2•eIF2B•ISRIB (6O85); phosphorylated eIF2 α •eIF2B (6O9Z). All structural figures were generated with UCSF Chimera (36) and BLENDER (<http://www.blender.org>).

GDP exchange assay

We modified the procedure to establish a loading assay for fluorescent GDP as described (1). Purified eIF2 (200 pmol) was incubated with a molar equivalent Bodipy-FL-GDP (Thermo Fisher Scientific) in assay buffer (20 mM HEPES, pH 7.5, 100 mM KCl, 5 mM MgCl₂, 1 mM TCEP, 0.1% NMP, and 1 mg/ml bovine serum albumin) to a volume of 18 μ l in 384 square-well black-walled, clear-bottom polystyrene assay plates (Corning). The reaction was initiated by addition of 2 μ l of buffer or purified wild-type and mutant eIF2B($\beta\gamma\delta\epsilon$) (2 pmol) under various conditions to compare nucleotide exchange rates. For comparison of tetramer or ISRIB-assembled octamer, eIF2B($\beta\gamma\delta\epsilon$) (2 pmol) was preincubated in 0.1% NMP and 2 mM ISRIB for 15 min before 10-fold dilution into the final reaction. These concentrations of vehicle and ISRIB were used throughout unless otherwise specified. Fluorescence intensity for both loading and unloading assays was recorded every 10 seconds for 60 or 100 minutes using a TECAN M1000 Pro plate reader (excitation wavelength: 495 nm, bandwidth 5 nm, emission wavelength: 512 nm, bandwidth: 5 nm). Data collected were fit with a first-order exponential equation.

Negative Stain collection and 2D Classification

Decameric eIF2B($\alpha\beta\gamma\delta\epsilon$)₂ + eIF2($\alpha\beta\gamma$) + ISRIB: eIF2B($\alpha\beta\gamma\delta\epsilon$)₂ was diluted to 800 nM eIF2B, eIF2 to 2 μ M, and a stock solution of 200 μ M ISRIB in N-methyl-2-pyrrolidone (NMP) was added to a final ISRIB concentration of 2 μ M in a final solution containing 20 mM HEPES-KOH, pH 7.5, 100 mM KCl, 1 mM TCEP, 5 mM MgCl₂, 0.1% NMP, and incubated on ice for 10 min. EM grids of negatively stained sample were prepared by applying 4 μ L of sample to a 400 mesh copper grid covered with continuous carbon film and stained with 2 % (w/v) uranyl formate, following the established procedure (42). Negative-stain EM grids were imaged on a FEI Tecnai T20 microscope (Thermo Fisher Scientific, US) operated at 200kV and equipped with a TVIPS TemCam F816 (8K 8K) scintillator based CMOS camera (TVIPS, Germany). Images were recorded at a nominal magnification of 50,000 \times , corresponding to a pixel size of 1.57 \AA at specimen level, and with a defocus set to 1.2 μ m.

References

1. H. P. Harding *et al.*, *Mol. Cell.* **11**, 619–33 (2003).
2. L. R. Palam, T. D. Baird, R. C. Wek, *J. Biol. Chem.* **286**, 10939–10949 (2011).
3. K. M. Vattem, R. C. Wek, *Proc. Natl. Acad. Sci.* **101**, 11269–11274 (2004).
4. K. Kashiwagi *et al.*, *Nature.* **531**, 122–125 (2016).
5. Y. Gordiyenko *et al.*, *Nat. Commun.* **5**, 3902 (2014).
6. B. Kuhle, N. K. Eulig, R. Ficner, *Nucleic Acids Res.* **43**, gkv930 (2015).
7. K. Dev *et al.*, *Mol. Cell. Biol.* **30**, 5218–33 (2010).
8. G. D. Pavitt, K. V Ramaiah, S. R. Kimball, A. G. Hinnebusch, *Genes Dev.* **12**, 514–26 (1998).
9. S. R. Kimball, J. R. Fabian, G. D. Pavitt, A. G. Hinnebusch, L. S. Jefferson, *J. Biol. Chem.* **273**, 12841–5 (1998).
10. T. Krishnamoorthy, G. D. Pavitt, F. Zhang, T. E. Dever, A. G. Hinnebusch, *Mol. Cell. Biol.* **21**, 5018–5030 (2001).

11. C. Sidrauski *et al.*, *Elife*. **2** e00498 (2013).
12. C. Sidrauski *et al.*, *Elife*. **4** e07314 (2015).
13. Y. Sekine *et al.*, *Science*. **348**, 1027–30 (2015).
14. A. Chou *et al.*, *Proc. Natl. Acad. Sci. U. S. A.* **114**, E6420–E6426 (2017).
15. M. Halliday *et al.*, *Cell Death Dis.* **6**, e1672 (2015).
16. Y. L. Wong *et al.*, *bioRxiv*, 462820 (2018).
17. J. C. Tsai *et al.*, *Science*. **359**, eaaq0939 (2018).
18. A. F. Zyryanova *et al.*, *Science*. **359**, 1533–1536 (2018).
19. R. A. de Almeida *et al.*, *PLoS One*. **8**, e53958 (2013).
20. T. Ito, A. Marintchev, G. Wagner, *Structure*. **12**, 1693–1704 (2004).
21. S. Dhaliwal, D. W. Hoffman, *J. Mol. Biol.* **334**, 187–195 (2003).
22. B. Eliseev *et al.*, *Nucleic Acids Res.* **46**, 2678–2689 (2018).

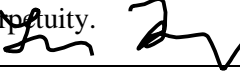
23. V. Beilsten-Edmands *et al.*, *Cell Discov.*, **1** 15020 (2015).
24. E. Dubiez, A. Aleksandrov, C. Lazennec-Schurdevin, Y. Mechulam, E. Schmitt, *Nucleic Acids Res.* **43**, 2946–2957 (2015).
25. T. Boesen, S. S. Mohammad, G. D. Pavitt, G. R. Andersen, *J. Biol. Chem.* **279**, 10584–10592 (2004).
26. J. Wei *et al.*, *Protein Cell.* **1**, 595–603 (2010).
27. R. Elsby *et al.*, *J. Virol.* **85**, 9716–25 (2011).
28. G. D. Pavitt, W. Yang, A. G. Hinnebusch, *Mol. Cell. Biol.* **17**, 1298–313 (1997).
29. C. R. Vazquez de Aldana, A. G. Hinnebusch, *Mol. Cell. Biol.* **14**, 3208–22 (1994).
30. A. Crespillo-Casado *et al.*, *J. Biol. Chem.* **293**, 7766–7776 (2018).
31. S. Q. Zheng *et al.*, *Nat. Methods.* **14**, 331–332 (2017).
32. K. Zhang, *J. Struct. Biol.* **193**, 1–12 (2016).
33. A. Punjani, J. L. Rubinstein, D. J. Fleet, M. A. Brubaker, *Nat. Methods.* **14**, 290–296 (2017).
34. T. Grant, A. Rohou, N. Grigorieff, *Elife.* **7** (2018), doi:10.7554/eLife.35383.

35. E. F. Pettersen *et al.*, *J. Comput. Chem.* **25**, 1605–1612 (2004).
36. A. Simonetti *et al.*, *Mol. Cell.* **63**, 206–217 (2016).
37. P. Emsley, B. Lohkamp, W. G. Scott, K. Cowtan, *Acta Crystallogr. Sect. D Biol. Crystallogr.* **66**, 486–501 (2010).
38. P. D. Adams *et al.*, *Acta Crystallogr. Sect. D Biol. Crystallogr.* **66**, 213–221 (2010).
39. V. B. Chen *et al.*, *Acta Crystallogr. Sect. D Biol. Crystallogr.* **66**, 12–21 (2010).
40. S. J. Ludtke, *Methods Enzymol.* **579**, 159–89 (2016).

Publishing Agreement

It is the policy of the University to encourage the distribution of all theses, dissertations, and manuscripts. Copies of all UCSF theses, dissertations, and manuscripts will be routed to the library via the Graduate Division. The library will make all theses, dissertations, and manuscripts accessible to the public and will preserve these to the best of their abilities, in perpetuity.

I hereby grant permission to the Graduate Division of the University of California, San Francisco to release copies of my thesis, dissertation, or manuscript to the Campus Library to provide access and preservation, in whole or in part, in perpetuity.

Author Signature  Date 09/12/2019